

# The Influence of In Vitro Degradation on the Properties of Polylactic Acid Electrospun Fiber Mats

Kardo Khalid Abdullah <sup>1</sup>  and Kolos Molnár <sup>1,2,3,\*</sup> 

<sup>1</sup> Department of Polymer Engineering, Faculty of Mechanical Engineering, Budapest University of Technology and Economics, Műegyetem rkp. 3, H-1111 Budapest, Hungary; [abdullahk@pt.bme.hu](mailto:abdullahk@pt.bme.hu)

<sup>2</sup> HUN-REN-BME Research Group for Composite Science and Technology, Műegyetem rkp. 3, H-1111 Budapest, Hungary

<sup>3</sup> MTA-BME Lendület Sustainable Polymers Research Group, Műegyetem rkp. 3, H-1111 Budapest, Hungary

\* Correspondence: [molnar@pt.bme.hu](mailto:molnar@pt.bme.hu)

**Abstract:** The scope of our study was to investigate the changes in electrospun polylactic acid (PLA) fiber mats' morphological, mechanical, and thermal properties in vitro. We electrospun two sets of PLA fiber mats with different average diameters, E6 (747 nm) and E10 (1263 nm). The degradation study of PLA electrospun fibers was carried out in phosphate-buffered saline solution at 37 °C to simulate conditions within the human system. The results reveal the thicker fibers (E10) degraded more rapidly than the E6 sample due to their different morphology. E10 showed a 29% reduction in diameter and a 41% weight loss, while E6 exhibited an 18% reduction in diameter and a 27.5% weight loss. E6's Young's modulus increased by 3.55 times, while E10's rose by 2.23 times after 28 days of degradation, and the fibers became more rigid. E6 showed a more pronounced decrease in crystallinity compared with E10. Changes in electrospun fiber diameters and crystallinity greatly influence the degradation mechanism of PLA.

**Keywords:** electrospinning; polylactic acid; polymer degradation; fiber mat



Academic Editor: Ramiro Rafael Ruiz Rosas

Received: 30 September 2024

Revised: 11 December 2024

Accepted: 25 December 2024

Published: 28 December 2024

**Citation:** Abdullah, K.K.; Molnár, K. The Influence of In Vitro Degradation on the Properties of Polylactic Acid Electrospun Fiber Mats. *Fibers* **2025**, *13*, 1. <https://doi.org/10.3390/fib13010001>

**Copyright:** © 2024 by the authors. Licensee MDPI, Basel, Switzerland. This article is an open access article distributed under the terms and conditions of the Creative Commons Attribution (CC BY) license (<https://creativecommons.org/licenses/by/4.0/>).

## 1. Introduction

Electrospinning (ES) is a flexible fabrication technique that produces ultrafine fibers from polymer solutions, typically in the nanometer to micrometer range [1,2]. The electrospun nanofiber mats have unique features, including high surface area [3], substantial porosity [4], and exceptional absorption capabilities [5]. Hence, ES is the most popular way to produce nanofibers from biopolymers both in academia and industry.

Electrospun nanofibers produced from biopolymers are extensively used in biomedical fields, such as tissue engineering and drug delivery [6–11]. Common biopolymers used in electrospinning include poly(caprolactone) (PCL), poly(ethylene glycol) (PEG), poly(lactic acid) (PLA), poly(lactic-co-glycolic acid) (PLGA), chitosan, and gelatin, due to their biocompatibility and biodegradability within the human body [12,13]. These biopolymers are favored because they do not cause harmful reactions or toxicity when in contact with living tissues, cells, or organisms [14,15] and are naturally biodegradable [16,17].

Before biopolymer fibers can be used in biomedical applications, it is essential to ensure they meet the required biocompatibility, biodegradability, and functionality standards [18]. The lifespan of the fibers in the body and their potential impact on surrounding cells and tissues must be completely known [19,20].

Among synthetic polymers, PLA is an eco-friendly option, widely favored by researchers, and commonly used in various applications [21–23]. It is produced through poly-

condensation of lactic acid, derived from the fermentation of carbohydrates found in various types of grains [24]. PLA has fair mechanical properties [25,26] and is handy for forming micro- or nano-sized fibers with precisely controlled surface and internal structures [27]. PLA readily undergoes hydrolysis within living organisms, producing lactic acid, which can be enzymatically degraded within the body, thus enhancing biocompatibility [28].

Based on the research findings of Katila et al. [29] and Anderson et al. [30], PLA undergoes natural environmental degradation, breaking down into carbon dioxide and water, contributing to its degradability. Furthermore, PLA can be easily synthesized, giving it a high potential in bioengineering applications [31]. Altogether, those unique characteristics of PLA electrospun nanofibers make them fit for applications where they can safely interact with the body and degrade without causing harm over time. Furthermore, their adjustable properties enable customization to fulfill specific medical requirements.

The elements influencing the degradation rates of biopolymers center around material properties, including molecular weight and distribution [32], the degree of crystallinity [33], porosity and pore size, shape, and morphology [34], and polymer composition [35]. In the crystalline polymer, the hydrolysis process takes place in both amorphous and crystalline regions at different rates [36], as shown in Figure 1. Several researchers have documented the degradation rates of various biopolymers under different conditions and timeframes.

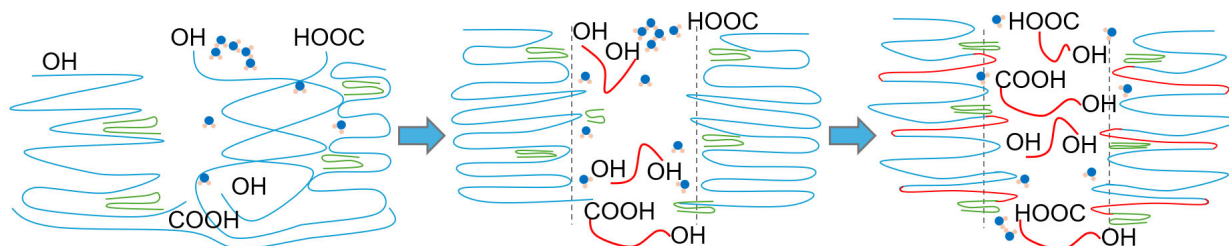


**Figure 1.** Hydrolysis process in PLA's amorphous and crystalline regions (long PLA chains: blue lines, short PLA chains: red lines, and OLA: green lines). This figure is based on the work by A Leonés et al., titled *In Vitro Degradation of Plasticized PLA Electrospun Fiber Mats: Morphological, Thermal and Crystalline Evolution*, and is licensed under the Creative Commons Attribution 4.0 International License (CC BY 4.0). This figure is reprinted; the original work can be found in [36].

Nowadays, the most preferable method involves testing biopolymer *in vitro* in a simulating condition, simulating enzymatic activity similar to that found in the living body. PLA has been frequently examined in PBS (phosphate-buffered saline) solution due to its ability to mimic the physiological conditions of the human body. Alternatively, other buffer solutions such as Tris-HCl, carbonate buffers, and sodium hydroxide are also used to simulate the diverse pH conditions present in different tissues and organs [37,38]. This assessment helps researchers understand how biopolymers engage with bodily surroundings, including pH, ionic strength, and osmolarity.

*In vitro* studies provide fundamental visions into biopolymer compatibility, degradation, and performance in actual biological states. The study by You et al. [39] concerns the *in vitro* degradation of electrospun PLA fibers (100–600 nm diameters) immersed in a PBS solution by measuring weight loss over 45 days. They evaluated the degradation by assessing the electrospun fiber mat weight reduction before and after the degradation test. The outcomes revealed no notable change in the weight of PLA electrospun fibers throughout that degradation period. Bogdanova et al. [40] observed that the weight loss of PLA *in vitro* degradation was approximately 7% after two weeks and around 8% after both 4 and 6 weeks.

The diameter and structure of electrospun fibers also change during the decomposition. Leonés et al. [36] experimented with immersing electrospun PLA fibers in a PBS solution. The average diameter decreased from 904 nm to 604 nm after 1 day. The most significant reduction was observed after 7 days, with the diameter dropping to 469 nm, representing a 48% decrease. This reduced size remained relatively stable up to 84 days. In addition to fiber diameters, hydrolytic degradation also affects the membrane porosity of fiber mats. Dias et al. [41] observed that hydrolytic degradation of electrospun PLLA mats leads to changes in fiber thickness and porosity. As the degradation advances, the fibers thicken, and the porosity decreases, resulting in a denser packing of fibers, likely due to the release of internal stresses.

Moreover, the thermal properties of fiber mats undergo alterations throughout the degradation process. Zong et al. [42] studied the degradation of electrospun poly(glycolide-co-lactide) (PLA10GA90) membranes in a 37 °C PBS solution over 12 days. They observed three distinct phases in  $T_g$ : a sharp rise in the first two days, a gradual decline, and a slow increase after six days. Since the glass transition temperature of PLA10GA90 was close to the incubation temperature, the initial rise in  $T_g$  was due to increased restraints on the amorphous chains after one day. In the second phase, hydrolysis caused more chain scissions in the amorphous regions, increasing chain mobility and decreasing  $T_g$ . However, the 12-day degradation period may not be adequate to fully capture variations in  $T_g$  as substantial changes in thermal properties could persist beyond this timeframe due to the slow kinetics of polymer chain scission and crystallization.

Li et al. [43] examined how electrospun PLGA membranes degrade in a PBS solution using clamps in a tensile testing device to assess the mechanical properties under stress. Their results show that the elastic modulus of unloaded electrospun membranes remained nearly constant, while that of loaded PLGA increased by approximately 5.5 times during the first week. Additionally, the ultimate strength rose from about 3.5 MPa to 10.1 MPa in the first week but steadily declined, disappearing completely after the seventh week. However, it is important to note that this experiment involved applying a creep stimulus to the samples. Therefore, not only did degradation occur, but creep was also a factor, and testing the samples after varying periods of creep was not considered when evaluating the results. By introducing such a stimulus, the assessment may not accurately reflect the actual mechanical characteristics, as the creep modulus tends to decrease over time under sustained loading.

The exact decomposition process of electrospun biopolymer mats is unclear due to their thin 2D fiber structure. Since variations in fiber diameter alter surface-area-to-volume ratios, it may affect degradation rates. Additionally, there needs to be more data on how quickly the mechanical properties of these fibers change during degradation. Consequently, the primary issue lies in the difficulty of handling electrospun fibers as specimens for testing tensile strength due to their delicate and refined structure, making them prone to damage or distortion during treatment. Furthermore, researchers have infrequently investigated how variations in degradation rates over short periods affect electrospun nanofibers' morphology and weight loss based on different surface-area-to-volume ratios. A complete understanding of how these variations affect thermal properties is important (i.e., glass transition temperature and degree of crystallinity).

In this study, we investigate the impact of degradation on the properties of PLA electrospun fiber mats over time, depending on their morphology in a simulated medium. Specifically, we analyze PLA fibers of two different diameters to observe their degradation behavior, monitoring changes in fiber morphology, weight, and mechanical and thermal properties at various time points. We hypothesize that the diameter of the fibers will significantly influence the degradation rate and mechanical performance, with larger fibers

exhibiting slower degradation and more stable properties due to their reduced surface-area-to-volume ratio. By monitoring these properties, we aim to gain insights into how variations in fiber structure affect their behavior during *in vitro* degradation.

## 2. Materials and Methods

### 2.1. Materials

Poly(lactic acid) (PLA) (2003D, MW = 159,000 g/mol) from Nature Works LLC (Plymouth, MN, USA) was used in this study to prepare polymer solutions. We dissolved PLA2003D pellets into chloroform (Azure Chemicals, Budapest, Hungary) and dimethylformamide (DMF) (Azure Chemicals, Budapest, Hungary) solvents at a 4:1 (*w/w*) ratio [44]. To investigate the effect of solution concentration on fiber diameter, two concentrations were prepared: 6%wt and 10%wt. This aims to produce fibers with diverse scales since the diameter of the fibers increases significantly with increasing polymer solution concentration [44,45]. We homogenized the polymer solution with a magnetic stirrer at 400 rpm at room temperature for 24 h.

### 2.2. Methods

Our study presents a detailed method involving electrospinning, *in vitro* degradation, and various characterization techniques to explore the variation in PLA electrospun fiber before and after degradation. We started by electrospinning each polymer solution (detailed in Section 2.2.1) to fabricate nanofiber mats with two different mean diameters. The fiber mats are immersed in a PBS solution held at 37 °C to assess how they degrade under simulated biological conditions. We analyzed these fiber mats using several methods, including scanning electron microscopy (SEM) to examine morphological changes, differential scanning calorimeter (DSC) for thermal analysis, and tensile testing for mechanical properties. Furthermore, we measure the fibers' weight before and after degradation, comprehensively evaluating their durability and performance.

#### 2.2.1. Electrospinning

We prepared a custom setup for the electrospinning process, as shown in Figure 2. The polymer solution was delivered from a 20 mL syringe to a 24G needle (with an inner diameter of 0.31 mm and an outer diameter of 0.55 mm) using a silicone rubber tube. The syringe was controlled and connected to a syringe pump (Aitecs SEP-10S, Vilnius, Lithuania). The needle's tip was securely fixed with a bolt attached to the power supply to deliver high voltage. Placing the syringe in the pump, we secured the needle onto the electrospinning setup and connected it to the positive cable carrying voltage from the DC power supply (MA2000 NT 65/P, Nagykanizsa, Hungary). Once the solution reached the spinneret's tip, we switched on the power supply at a voltage of 16 kV, simultaneously pumping the solution at a rate of 3 mL/h. The process ran through the room temperature (25 °C) and relative humidity between 30% to 40%. The electrospun fiber placed on the grounded metallic collector is covered with taped aluminum foil for easier handling and sample storage. The collector is positioned 20 cm away from the needle's tip. We collected each sample for 45 min. Subsequently, the electrospun fiber mats were carefully removed from the aluminum foil. This entire procedure was repeated for all samples using the same parameters.

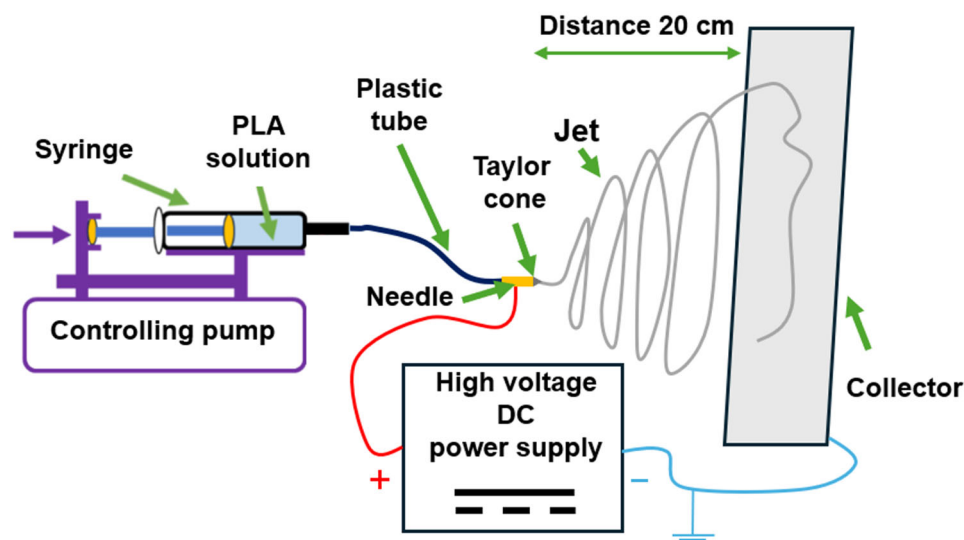


**Figure 2.** Electrospinning setup.

### 2.2.2. In Vitro Degradation

The in vitro degradation of electrospun PLA fibers was studied by exposing them to controlled conditions of temperature and pH. PLA degrades in PBS solution due to hydrolytic and chemical processes. Immersing PLA electrospun fibers in PBS solution simulates biological conditions similar to those in the human body, enabling an assessment of fiber degradation over time. The PBS solution (pH 7.4) was prepared by dissolving salt tablets (P4417-Sigma-Aldrich, St. Louis, MO, USA) in distilled water following the manufacturer's mixing instructions. We replaced the PBS solution weekly to ensure the pH stayed stable throughout the experiment. Given the short duration, no significant pH changes were expected, as confirmed by previous studies [36].

Electrospun fiber samples (E6 and E10) were labeled according to their designated degradation periods (1, 3, 7, and 28 days) and immersed in the PBS solution. To maintain a consistent experimental temperature, the samples were placed in a sealed container and incubated in an incubator (IN-36DDI, Berlin, Germany) at 37 °C. After each degradation period, the fibers were removed, rinsed with distilled water three times to eliminate any byproducts and degraded particles, and then dried in a vacuum drying chamber (Binder VD 53, Tuttlingen, Germany) at 37 °C for 24 h before further analysis.

### 2.3. Characterization

Changes in fiber morphology, weight, mechanical properties, and thermal properties monitored PLA electrospun fiber mats' degradation rate and properties. We denote the samples of the two concentrations as E6 (6% PLA concentration) and E10 (10% PLA concentration).

#### 2.3.1. Scanning Electron Microscopy Analysis

The morphologies of electrospun fiber mat sets (E6 and E10) were observed by scanning electron microscopy (SEM, JEOL 6380 LA, Tokyo, Japan) throughout the degradation process for each period. We prepared samples from both fiber mats by fine-coating them with gold (Au) for 30 s in an evacuated chamber. SEM images were taken, and 100 fibers were randomly chosen to measure their diameters using ImageJ software (version 1.54g, National Institutes of Health, Bethesda, MD, USA). The average diameter, standard deviation, and frequency distributions were calculated.

### 2.3.2. Fiber Weight Loss

To evaluate the weight loss of electrospun fiber mats during the degradation process, we recorded the weight of 16 fiber mat specimens for each period. Specimens cut in (length~20 mm, width~4 mm) and weighed before and after degradation (dried). We measure the specimen's weight using a high-precision laboratory scale (Sartorius Lab Instruments GmbH-Quintix125D-1CEU, Göttingen, Germany). We calculated the weight loss of electrospun fibers using Equation (1):

$$WL (\%) = \frac{W_i (mg) - W_a (mg)}{W_i (mg)}, \quad (1)$$

where  $W_L$  (%) is the weight loss percentage,  $W_i$  is the weight of fiber mats before degradation, and  $W_a$  is the weight of fiber mats after degradation.

### 2.3.3. Thermal Characterization

During the degradation study, we determined the specimens' glass transition temperature ( $T_g$ ) and degree of crystallinity ( $\chi_c\%$ ). We used a differential scanning calorimeter (DSC) (DSC-Q2000-TA Instruments, New Castle, DE, USA) to measure thermal properties. We performed a DSC examination for each set of electrospun fiber mats (E6 and E10) before and within each period of in vitro degradation. We prepared specimens from electrospun samples (weighing 5–9 mg) and used aluminum pans for the measurements. Specimens were subjected to a heat–cool–heat cycle ranging from 25 °C to 200 °C at a heating rate of 10 °C/min. Notably, cold crystallization occurred during the heating process. Therefore, we needed to consider it in the calculations. The degree of crystallinity ( $X_c\%$ ) was calculated from the results of the first heating cycle using Equation (2). Finally, we compared the changes in  $T_g$  and  $X_c\%$  within the degradation process.

$$X_c\% = \frac{\Delta H_m - \Delta H_{cc}}{\Delta H_{tc}} \times 100 \quad (2)$$

where  $\Delta H_m$  is the melting enthalpy,  $\Delta H_{cc}$  is the cold crystallization enthalpy, and  $H_{tc}$  is the theoretical melting enthalpy of the completely crystalline polymer, taken to be 93 J g<sup>-1</sup> according to the literature [46].

### 2.3.4. Fourier Transform Infrared (FTIR) Spectroscopy

Fourier transform infrared (FTIR) spectroscopy was used to investigate the chemical structure and functional groups in the E6 and E10 electrospun fiber mats within in vitro degradation. The analysis was conducted using a Tensor II FTIR spectrometer (Bruker, Billerica, MA, USA). Spectra were obtained in attenuated total reflectance mode, with a resolution of 4 cm<sup>-1</sup>, spanning a wavelength range from 400 to 4000 cm<sup>-1</sup>.

### 2.3.5. Mechanical Characterization

We prepared tensile test specimens from electrospun fiber mats to measure their mechanical properties. We cut and peeled off the electrospun fiber mats from the aluminum foil and made strips (4 ± 1 mm wide and 20 ± 2 mm long) carefully to avoid their damage. We prepared fifteen specimens for each set of electrospun fiber mats for each period to improve accuracy and consistency. Since it is challenging to handle fiber mat specimens for tensile tests within a hydrolysis medium due to their delicate and fine structure, we securely affixed them to a polyethylene terephthalate (PET) frame holder using electrical insulation tape. PET does not readily degrade in PBS solution and remains stable in such environments.

The frame holder (dimension: 20 mm by 45 mm) features an opening in the middle (dimension: 10 mm by 25 mm), as shown in Figure 3a. Additionally, we designed a sample holder to ensure that all electrospun fiber mats remain separate and intact when immersed in the PBS solution, as shown in Figure 3b,c.

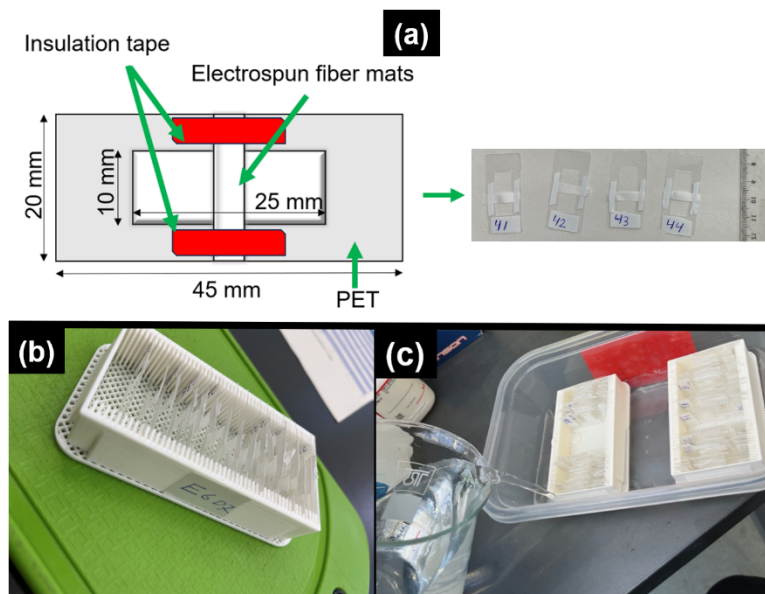


**Figure 3.** (a) Electrospun specimens for tensile test in PET frame holder, (b) placing the fiber mat samples into a sample holder, and (c) immersing them in hydrolysis medium.

The tensile strength, Young's modulus, and strain of specimens were determined using a Zwick Z005 device (Zwick Roell, Ulm, Germany) with a 20 N load cell. Fiber mats from the frame holder were secured between the tensile machine clamps to ensure the fiber mat specimens were straight and perpendicular to the horizontal surface of the clamps. After the specimens were fixed in place, the sides of the frame holder were cut to avoid affecting the results. The stretching rate was 10 mm/min, with an initial length between the clamps of 20 mm at room temperature (25 °C) and humidity of  $35 \pm 5\%$ . In addition, we weighed each specimen before and after the immersion period.

When calculating the cross-section of the specimens, we estimated the real cross-section ( $A$ ), i.e., the sum of the cross-sections of the nanofibers only. We performed this from the linear density of the specimen using Equation (3).

$$A = \frac{m}{l \times \rho} \quad (3)$$

where  $m$  is the weight of the electrospun specimen (mg),  $l$  is the length of the specimen (mm),  $\rho$  is the density of the polymer ( $1240 \text{ kg/m}^3$  according to the technical datasheet). We assumed that the specimen's cross-section is the same along the length of the specimen.

### 3. Results and Discussion

#### 3.1. SEM Analysis

We aimed to produce fiber mats with different diameters, and we expected that E10 would produce thicker fibers than E6 based on the literature and the preliminary experiments.

SEM analysis revealed that the E6 fibers had an average diameter of 747 nm, while the E10 fibers were significantly thicker at 1263 nm, approximately 70% larger, as shown in Figure 4. The observed increase in diameter for the E10 fibers is attributed to the higher viscosity of the solution, which reduced the stretching and elongation of polymer jets

during electrospinning [47]. Therefore, the higher polymer concentration promoted the production of thicker nanofibers, consistent with findings in the literature [48].

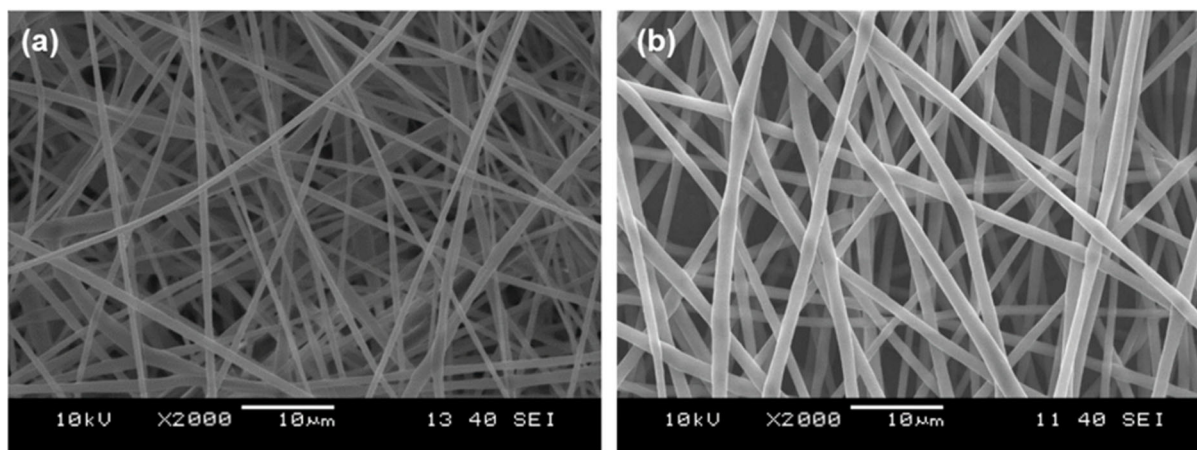


**Figure 4.** SEM images of PLA electrospun fibers (a) E6 and (b) E10.

During the degradation, the E6 and E10 electrospun fiber mats' diameters underwent significant changes, as shown in Figure 5. The average fiber diameter of the E6 fiber mats initially decreased from its original size to 740 nm after 1 day, reflecting a reduction of approximately 5.5%. This slight change indicates the onset of surface erosion. After 3 days, the diameter further reduced to 18.4%. Since PLA undergoes biosorption predominantly through bulk erosion [49]. This reduction in diameter could be attributed to the infiltration of water molecules into the fibers. Hydrolysis breaks down high molecular weight polymers into oligomers, increasing carboxyl groups, which enhances water diffusion, as reported in the literature [50]. The fibers then experienced a temporary increase to 13% increase from the 3-day measurement due to water absorption, which caused them to swell before continuing to degrade. Ultimately, the average fiber diameter decreased to 18.8% from the 7-day measurement. While random sampling introduces some errors and may result in artifacts from the random deposition of fibers, the decreasing trend in fiber diameters is still clearly visible.

The E10 fiber mats exhibited a significantly higher initial reduction in mean diameter after just one day of degradation than the E6 fiber mats. The E10 fibers showed a notable decrease after three days as degradation continued, indicating rapid degradation likely driven by increased water uptake. After seven days, the average diameter of the E10 fibers increased, followed by a decrease after 28 days, similar to the behavior observed in the E6 fiber mats. Various factors can explain the changes in fiber diameter observed during the degradation process. The E10 fibers went through a more considerable initial decrease.

Moreover, we analyzed diameter frequency counts before and after degradation among 100 randomly selected fibers. The E6 fibers primarily ranged from 400 to 800 nm before degradation, with significant reductions observed after 28 days, leading to most fibers falling below 1 micrometer. In contrast, the E10 fibers had no diameters below 700 nm initially, but after 28 days, all fibers larger than 1400 nm disappeared, and more than half were reduced to below 1 micrometer, showing a similar trend.

Since the E6 fibers have a higher surface area relative to their volume, this allows them to expose more surface to the degradation medium for a more uniform and efficient breakdown, causing the fibers to fragment and weaken. After 28 days of degradation, we noticed some of the E6 fibers had broken due to rapid surface erosion, as shown in Figure 6. Therefore, we did not extend the investigation to longer periods due to the significant structural damage observed in the fiber mats on day 28.

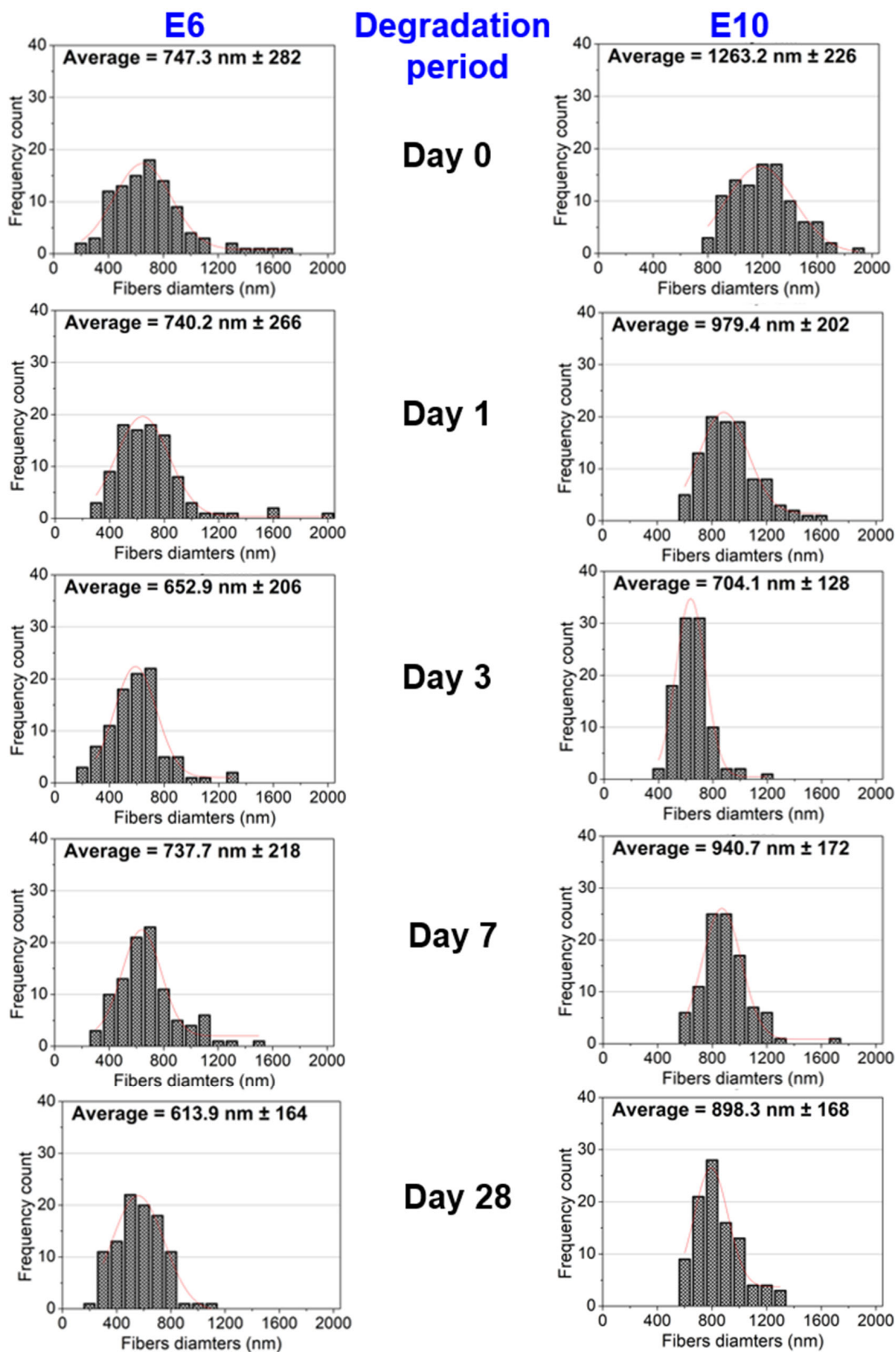


**Figure 5.** Change in fibers frequency count and average diameters of E6 and E10 electrospun fibers before and after degradation.

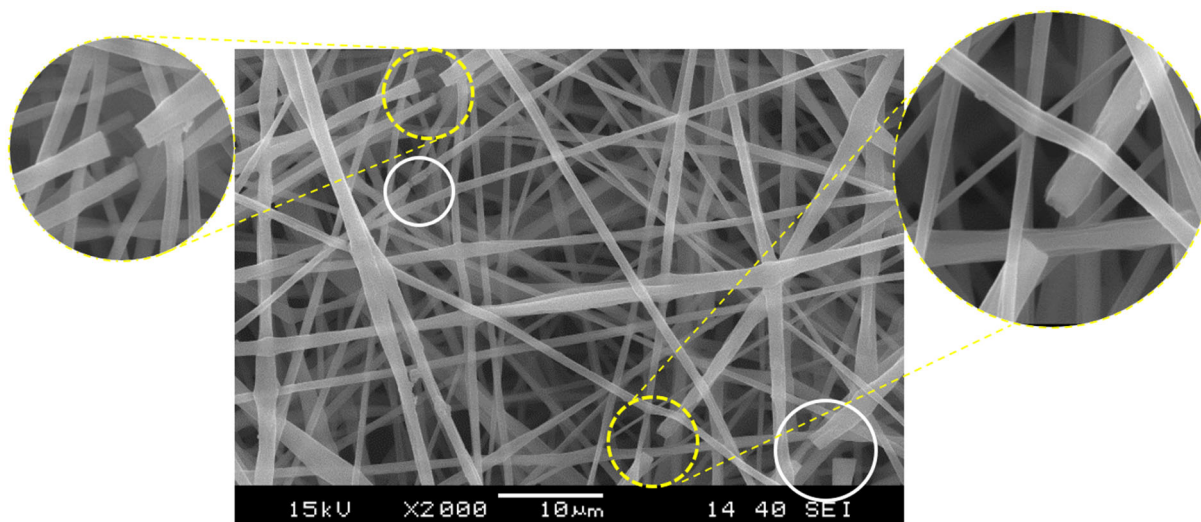


**Figure 6.** PLA electrospun fibers broke after 28 days of degradation. White circles highlight defect regions, while yellow dashed lines indicate zoomed-in areas for detailed visualization.

### 3.2. Weight Loss

The degradation behavior of the E6 and E10 electrospun fiber mats displayed distinct forms, mainly influenced by their structural differences. The weight loss of the E6 and E10 electrospun fibers is shown in Figure 7. Initially, the E6 fibers showed an unexpected increase in weight, gaining 3.8% after 1 day and 5.6% after 3 days of degradation. This weight gain is primarily attributed to the accumulation of hydrophilic byproducts (i.e., low molecular weight oligomers and lactic acid) in fiber mats due to degradation in saline solution. Despite thorough washing, these byproducts might remain trapped in the fibers, leading to water retention. As the E6 fiber mats degraded, new hydrophilic groups like carboxylic acids formed on the fiber surface, further increasing water absorption. Since fiber mats have extensive surface area and a greater presence of hydrophilic groups, the fibers can take up a substantial amount of moisture quickly. Since the samples were weighed the day after drying, this may account for the mass gain noted in both samples at the 3-day measurement. After 7 days, the E6 fiber mats lost weight (8%) as degradation progressed, and by 28 days, they had lost 27.5% of their initial weight.

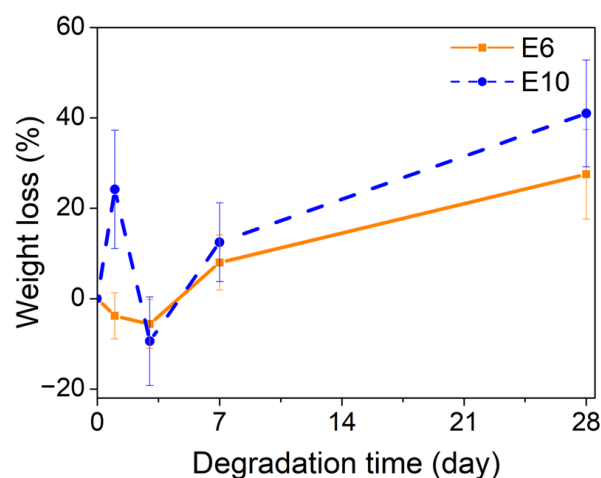


**Figure 7.** Weight loss of E6 and E10 electrospun fiber mats as a function of degradation time.

On the other hand, the E10 fibers followed a different path within the degradation periods. After just 1 day, they lost a significant 24.2% of their weight, likely because

their thicker surface degraded faster than the interior, leading to an initial mass loss. By day 3, though, the E10 fibers showed a brief weight gain of 9.4%, similar to the E6 fibers, likely due to water retention. After this, the degradation picked up again, with the fibers losing 12.5% of their weight by day 7. After 28 days of degradation, the E10 fiber mats had lost 41% of their weight, compared with just 27.5% for the E6 fiber mats. The high standard deviation in measuring the weight of fiber mats is largely attributed to sample heterogeneity, crystallinity, differences in moisture absorption, and weighing precision. Overall, the results show that the E6 fibers degraded more slowly over time, while the E10 fibers experienced a quicker and more significant weight loss. This clearly shows how the morphology of PLA electrospun fiber mats affected their degradation properties.

### 3.3. Thermal Properties

We determined the electrospun fibers' thermal properties from the DSC measurements. The fibers from each group displayed different behavior during the investigated degradation periods. Additionally, we analyzed the results from the first heat cycle of the DSC curves for PLA granules as references and both groups of electrospun fibers (E6 and E10) over the degradation periods, as depicted in Figure 8.

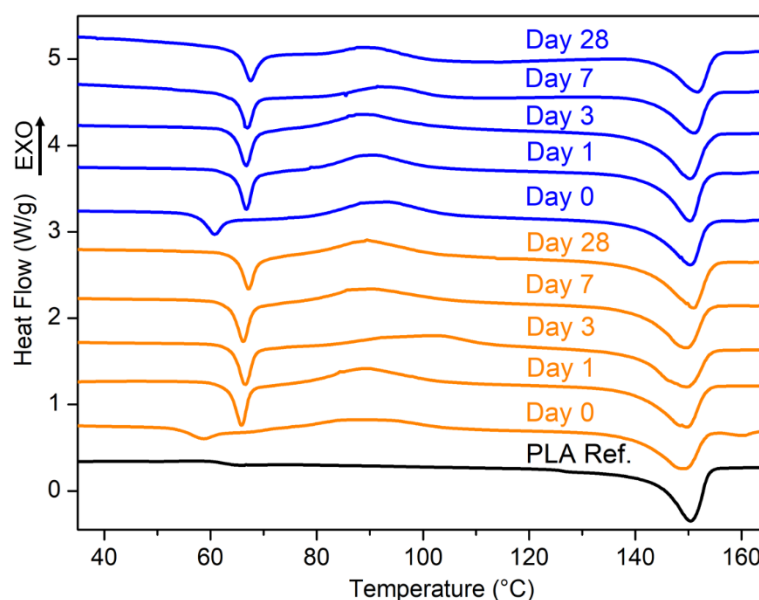


**Figure 8.** DSC curve: the black line represents PLA granules as reference, the orange line represents E6 electrospun fibers, and the blue line represents E10 electrospun fibers (number of days represents period of in vitro degradation).

We calculated the degree of crystallinity ( $X_c\%$ ) and glass transition temperature ( $T_g$ ) from the DSC curves, as shown in Figure 9. PLA granules, as references, displayed a higher  $T_g$  (61.97 °C) and  $X_c\%$  (34.18%) from electrospun fibers E6 and E10, highlighting the influence of ES processing techniques on the thermal properties of PLA. The lower crystallinity is typically attributed to the solvent evaporation rate in the ES technique, which did not allow enough time for the electrospun fibers to form a highly crystalline structure in the final fibers [51,52]. On the other hand, E6 showed a lower  $T_g$  (56.4 °C) and  $X_c\%$  (8.5%) before the degradation, whereas E10 exhibited a higher  $T_g$  (59.0 °C) and  $X_c\%$  of (16.2). This difference in  $X_c\%$  is also due to smaller fibers tending to crystallize less, as their small diameter greatly limits the space available for crystal growth [53].

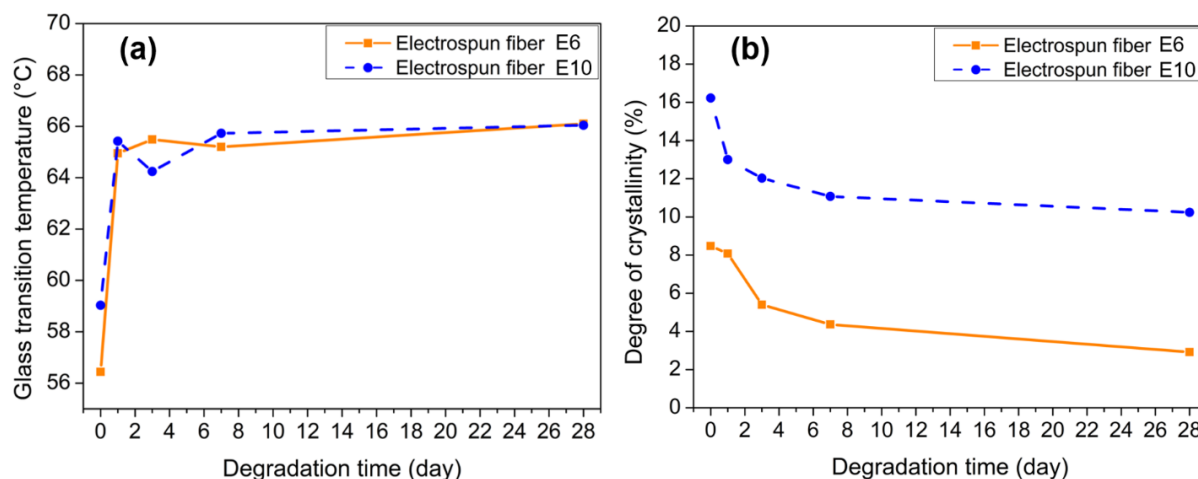


**Figure 9.** DSC results of electrospun fiber mats E6 and E10 before and after degradation (a) glass transition temperature and (b) degree of crystallinity.

Significant changes in thermal properties were noted upon exposure to *in vitro* degradation on different periods (1, 3, 7, and 28 days) for both types of samples. The  $T_g$  of the E6 fiber mats increased to 65.0 °C, with a reduction in  $X_c\%$  to 8.1%. This initial rise in  $T_g$  may be attributed to two factors. First, the beginning of hydrolytic degradation likely results in the creation of lower molecular weight chains. Second, during the electrospinning process, some solvents may have been trapped within the fibers, functioning as plasticizers [54].

Once the fibers were exposed to the degradation conditions, these solvents were washed out, contributing to the increase in  $T_g$ . After 3 days, electrospun fiber E6 underwent no significant changes in  $T_g$  but notable declines in  $X_c\%$ , indicating sustained degradation and crystallinity loss in the electrospun fibers. Similarly, for the E10 sample, after one day of degradation,  $T_g$  rose to 65.4 °C, while  $X_c\%$  decreased to 13%, suggesting similar considerations as in the E6 fibers. After 3 days of degradation, a slight decrease in  $T_g$  (64.2 °C) occurred. Nevertheless,  $T_g$  increased again during subsequent degradation periods (7 and 28 days), accompanied by decreases in  $X_c\%$ . The change in both the E6 and E10 fiber mats  $T_g$  occurs in three distinct phases: (1) a sharp increase at the onset of degradation, (2) a gradual decrease following the initial phase, and (3) a slow rise between 7 and 28 days of degradation, consistent with the literature findings [42]. These results present ongoing degradation and crystallinity loss of PLA electrospun fiber mats within degradation periods. A consistent decline in  $X_c\%$  indicates a continuous breakdown and shrinking of the fibers' crystalline structure, followed by further degradation in the crystalline region, as reported in the literature [39]. As noted in the literature, the increase in  $T_g$  is generally attributed to degradation progress since hydrolysis cuts the PLA macromolecules into shorter chains [55]. In particular, anything that restricts rotational motion within the chain increases the value of  $T_g$  [56]. Therefore, we analyzed the material by Fourier-transform infrared spectroscopy.

### 3.4. FTIR Analysis

Based on the FTIR results, changes in absorbance peak intensities are evident during the degradation process for both fiber mats (E6 and E10). In the case of PLA, the formation of carbonyl groups (C=O) occurs during the degradation, which enhances interaction with the polymer structure through the formation of weak hydrogen bonds [50,57,58], which restricts the mobility of the polymer chains, increases the  $T_g$ , and makes the fiber mats more rigid. Therefore, we focused on the absorbance intensities for key peaks: 1750  $\text{cm}^{-1}$ , representing carbonyl groups (C=O stretching) from ester bonds in PLA [59];

$\text{CH}_3$  and  $\text{CH}$  bending at around  $1450\text{ cm}^{-1}$  [60,61];  $\text{C-O}$  and  $\text{C=O}$  stretching at  $1080\text{ cm}^{-1}$  and  $1180\text{ cm}^{-1}$  [59,62]; and  $870\text{ cm}^{-1}$  peak (related to  $\text{C-C}$  stretching) [63,64], as shown in Figure 10.

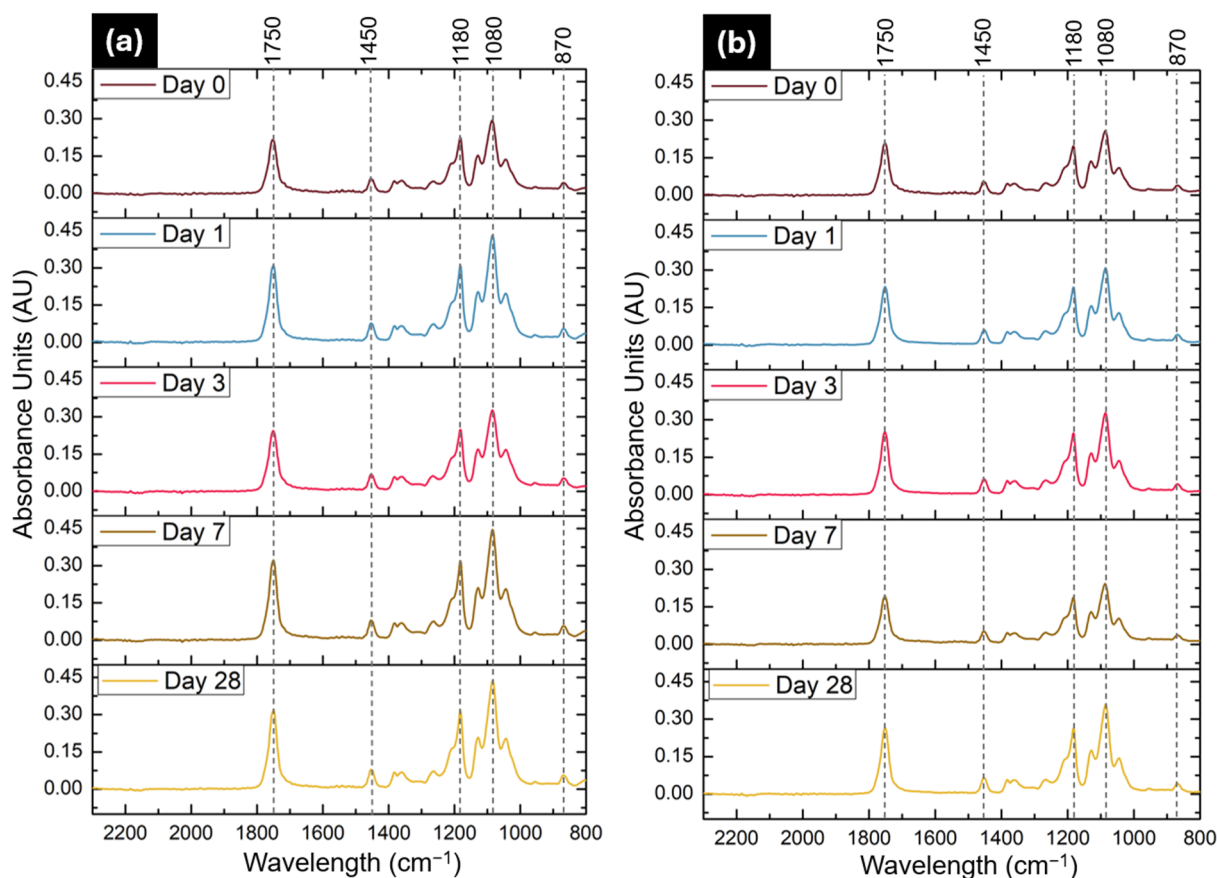


**Figure 10.** Peak absorbance intensities from FTIR spectra of (a) E6 fiber mats and (b) E10 fiber mats within a degradation period.

During the E6 and E10 fiber mat degradation, the key absorbance peaks show notable changes, particularly at  $1080\text{ cm}^{-1}$ ,  $1180\text{ cm}^{-1}$ , and  $1750\text{ cm}^{-1}$ , as shown in Table 1. For the E6 fiber mats, absorbance at the  $1750\text{ cm}^{-1}$  ( $\text{C=O}$  stretching) peak increased by 41% on day 1, decreased by 23% on day 3, and then rose by 33% on day 7, remaining unchanged by day 28. Following the same trends at  $1180\text{ cm}^{-1}$  peak increased by 41% on day 1, decreased by 19% on day 3, rose by 28% on day 7, and remained constant by day 28. For the peak at  $1080\text{ cm}^{-1}$ , absorbance increased by 43% on day 1, decreased by 23% on day 3, rose by 33% on day 7, and remained unchanged by day 28. All peaks underwent trends of increasing at the initiation of degradation, then decreasing on day 3, rising on day 7, and remaining constant until day 28. The initial increase in absorbance at these peaks is attributed to the formation of carbonyl groups ( $\text{C=O}$ ), commonly found in carboxylic acids. The subsequent decrease in absorbance suggests that some of these carbonyl interactions may have been disrupted due to degradation processes. The increase observed on day 7 indicates the formation of additional hydroxyl ( $-\text{OH}$ ) or stronger carbonyl interactions. In contrast, the stabilization on day 28 suggests that these processes have reached equilibrium. The  $870\text{ cm}^{-1}$  peak (linked to  $\text{C-C}$  stretching) and the  $1450\text{ cm}^{-1}$  peak (related to  $\text{CH}_3$  bending) show only minor shifts, suggesting these areas remain relatively unaffected.

**Table 1.** Key peaks absorbance intensities for E6 and E10 fiber mats within in vitro degradation.

Fiber Mats	Degradation Period (Days)	Absorbance Units at Peak 870 cm <sup>-1</sup>	Absorbance Units at Peak 1080 cm <sup>-1</sup>	Absorbance Units at Peak 1180 cm <sup>-1</sup>	Absorbance Units at Peak 1450 cm <sup>-1</sup>	Absorbance Units at Peak 1750 cm <sup>-1</sup>
E6	0	0.04	0.30	0.22	0.06	0.22
	1	0.05	0.43	0.31	0.08	0.31
	3	0.05	0.33	0.25	0.07	0.24
	7	0.06	0.44	0.32	0.08	0.32
	28	0.05	0.44	0.32	0.08	0.32
E10	0	0.04	0.26	0.20	0.05	0.21
	1	0.04	0.31	0.23	0.06	0.23
	3	0.04	0.33	0.25	0.06	0.25
	7	0.04	0.24	0.19	0.05	0.19
	28	0.04	0.36	0.26	0.06	0.27

In contrast, E10 exhibited similar trends, revealing an initial increase followed by decreases and eventual stabilization at the 1080 cm<sup>-1</sup>, 1180 cm<sup>-1</sup>, and 1750 cm<sup>-1</sup> peaks but no changes at peaks 870 cm<sup>-1</sup> and 1450 cm<sup>-1</sup> belonging to the backbone. However, the decreasing trends in E10 were primarily observed after 7 days of degradation. Since the E10 fibers were thicker and had a smaller surface-area-to-volume ratio than the E6 fibers, their degradation progressed more slowly. Furthermore, the E10 fibers showed limited evidence of carbonyl group formation, as indicated by the less absorbance at those peaks than the E6 specimens.

### 3.5. Mechanical Properties

From the tensile test, we obtained stress–strain curves for E6 and E10 before and after degradation in each period. A comparison of the fiber mats before and after 28 days of degradation shows significant changes in their mechanical properties, as depicted in Figure 11. The rest of the results (days 1, 3, 7) can be found in the Supplementary Material.

Both fiber mats demonstrate a notable shift toward lower strain at break, suggesting increased brittleness over time. This shift indicates a reduction in flexibility and ductility as the fibers degrade.

We calculated the average yield strength, strain at break, and Young’s modulus from the tensile testing results. The mechanical properties of electrospun mats before and after degradation are presented in Table 2.

The rate of change in Young’s modulus for both E6 and E10 increases over the degradation period. E6 shows a sharper initial rise in stiffness during the early phase (0–3 days), with a ~38% increase from day 0 to day 1, while E10 underwent a more modest 8% increase in the same period. However, E6 and E10 display the most significant increase in stiffness between days 7 and 28, with a ~60% rise. When comparing the overall Young’s modulus of the fiber mats before degradation and after 28 days, both E6 and E10 showed significant increases, with E6 exhibiting a more substantial change. E6’s modulus increased by approximately 3.55 times, while E10’s modulus rose by about 2.23 times after 28 days of degradation. This difference is attributed to the E10 fibers having a higher crystallinity than the E6 fibers, as greater crystallinity typically results in enhanced modulus and strength.

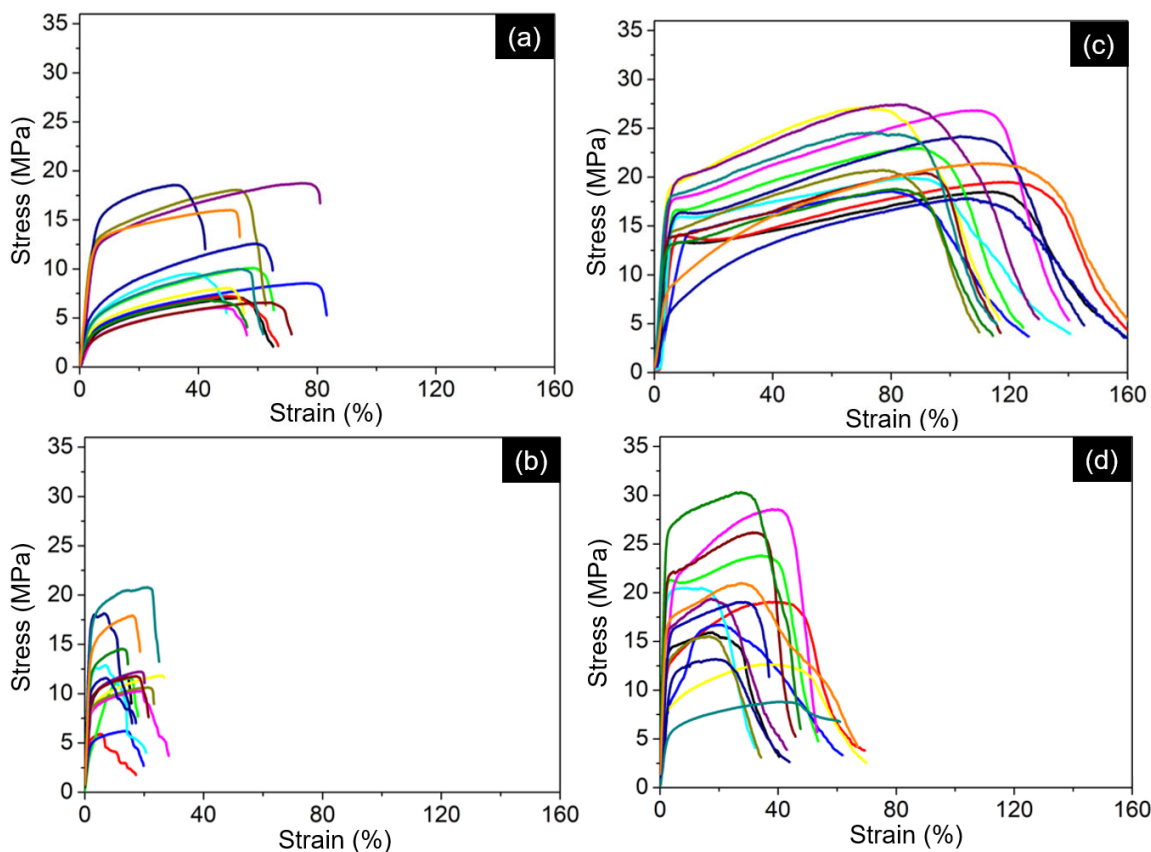


**Figure 11.** Stress–strain curves of electrospun fiber mats (different colors represent the result curves of each specimen): (a) E6 before degradation, (b) E6 after 28 days of degradation, (c) E10 before degradation, and (d) E10 after 28 days of degradation.

**Table 2.** Mechanical properties of electrospun fibers before and after in vitro degradation.

Electrospun Fiber Mat	Degradation Period (Days)	Young’s Modulus (MPa)	Strain at Break (%)	Yield Strength (MPa)
E6	0	168.6 ± 104.27	61.87 ± 10.85	10.93 ± 4.66
	1	232.6 ± 27.11	67.58 ± 13.77	17.06 ± 0.99
	3	293.7 ± 159.75	62.52 ± 16.51	19.56 ± 1.82
	7	373.86 ± 93.33	20.05 ± 6.43	9.62 ± 1.63
	28	598.72 ± 229.51	20.10 ± 4.08	12.54 ± 4.04
E10	0	316.48 ± 95.69	132.86 ± 20.91	21.91 ± 3.35
	1	341.58 ± 178.02	118.91 ± 26.24	20.84 ± 3.15
	3	416.71 ± 145.12	113.26 ± 36.53	25.95 ± 6.63
	7	439.03 ± 156.67	123.64 ± 17.85	20.26 ± 4.55
	28	706.92 ± 333.62	50.53 ± 12.78	19.37 ± 6.00

When comparing the yield strength of E6 and E10 electrospun fiber mats after one day of degradation, E6 experienced a substantial increase of 55.5%, while E10 saw a more modest rise of 18.6% after three days. This might be related to the water washing away the residual solvent from fibers, which can improve the mechanical properties. Later, degradation becomes the primary factor influencing the PLA fiber mats’ properties. Therefore, after seven days, E6’s yield strength dropped sharply by almost 50%, in contrast

to E10, which demonstrated a steadier decline of 21.9%. After 28 days, E6 showed a slight recovery, increasing by 30.3% from its value at seven days, whereas E10 maintained better structural integrity, gradually decreasing by 9.5%. From the results, E10 indicates a slower hydrolytic degradation after 28 days, where the denser network and higher molecular weight present resistance against the cleavage of polymer chains. In addition, the E10 fibers had roughly double the crystallinity of the E6 fibers. This happens because hydrolysis mainly reduces the number of tie chains in the non-crystalline area while having minimal impact on the overall molecular structure of the crystalline polymer [36,65].

Overall, the E6 fibers exhibited significant fluctuations in yield strength, while the E10 fibers displayed greater stability and resilience throughout the degradation process. The fiber mats exhibited variations in crystallinity, with E10 displaying a higher degree of crystallinity. Consequently, E6 underwent degradation at a faster rate. The residual solvent might act as a plasticizer. If the water washes away the solvent, that can improve the properties in the first few days.

Moreover, the strain at the break of the E10 fibers shows a higher initial and sustained strain, indicating better retention of flexibility and elasticity throughout the degradation process. Therefore, both E6 and E10 went through a dramatic reduction in strain during degradation. Fibers showed a significant loss of flexibility as degradation progressed. This is consistent with the degradation mechanism, leading to brittle material easily fracturing under stress. A decrease in the molecular weight causes a considerable reduction in the fiber's ability to stretch. Hence, it led to an increase in smaller, shorter polymer chains. These shorter chains form fewer entanglements and slide past each other more easily [66]. The results of mechanical changes in PLA fiber mats offer insights into how morphological scale fibers influence stability and longevity under degradation conditions.

#### 4. Conclusions

This study highlighted the changes in PLA electrospun fiber mat properties when subjected to *in vitro* conditions using a phosphate-buffered saline solution at 37 °C, simulating physiological conditions. PLA fibers with two different diameters were electrospun from 6% (E6) and 10% (E10) solutions. We employed various analytical techniques to gather valuable insights into the fibers. The key findings are summarized as follows:

- SEM images showed significant degradation and fiber fracturing after 28 days. The E6 fiber mats lost 27.5% of their weight, while the E10 fibers lost 41%. Differences in diameter contributed to the varying degradation rates between the two fiber types.
- DSC analysis indicated that non-degraded samples had a lower  $T_g$ , suggesting solvent trapping and a plasticizing effect. The  $T_g$  of PLA electrospun fiber mats initially increased due to hydrolytic degradation and solvent release, then gradually decreased and increased again. The degree of crystallinity continuously decreased, indicating ongoing degradation. FTIR analysis revealed that the E10 fibers degraded more slowly and formed fewer carbonyl groups than the E6 fibers, likely due to their thicker structure and lower surface-area-to-volume ratio.
- Mechanical tests confirmed that both the E6 and E10 fiber mats underwent significant changes during degradation. E6 showed a sharp rise in Young's modulus followed by a steep decline in yield strength after 7 days, while E10 exhibited more stability with slower degradation, showing a gradual decrease in yield strength and higher strain at break. After 28 days, E6's modulus increased 3.55 times, while E10's rose 2.23 times. The E10 fibers were more resistant to degradation, while the E6 fibers degraded faster and showed more significant changes in mechanical properties.

These findings offer valuable insights into the degradation of PLA fiber mats and their potential for biomedical applications. Understanding how fiber diameter and crystallinity affect degradation in tissue engineering will help design scaffolds that maintain strength during early tissue growth and degrade as new tissue forms. For bioresorbable implants, this study's insights into the mechanical properties and degradation behavior of PLA fibers will guide the development of implants that provide support during healing and degrade at the optimal rate, reducing the need for surgical removal.

**Supplementary Materials:** The following supporting information can be downloaded at: <https://www.mdpi.com/article/10.3390/fib13010001/s1>, Appendix S1. Electrospun fibers diameter measurements, Appendix S2. Weight loss measurements, Appendix S3. Stress-strain curves.

**Author Contributions:** Methodology, K.K.A. and K.M.; Software, K.K.A.; Validation, K.K.A. and K.M.; Formal analysis, K.K.A. and K.M.; Investigation, K.K.A. and K.M.; Data curation, K.K.A. and K.M.; Writing—original draft, K.K.A.; Writing—review & editing, K.K.A. and K.M.; Visualization, K.K.A. and K.M.; Supervision, K.M. All authors have read and agreed to the published version of the manuscript.

**Funding:** The research reported in this paper was supported by the National Research, Development and Innovation Office (FK 138501). Project no. TKP-9-8/PALY-2021 has been implemented with the support provided by the Ministry of Culture and Innovation of Hungary from the National Research, Development and Innovation Fund, financed under the TKP2021-EGA funding scheme. The research reported in this paper was supported by the H2020-MSCA RISE No. 872152-GREEN-MAP project of the European Union.

**Data Availability Statement:** Data will be made available on request.

**Acknowledgments:** Kolos Molnár was supported by the János Bolyai Research Scholarship of the Hungarian Academy of Sciences (MTA).

**Conflicts of Interest:** The authors declare no conflict of interest.

## References

1. Stramarkou, M.; Tzegiannakis, I.; Christoforidi, E.; Krokida, M. Use of Electrospinning for Sustainable Production of Nanofibers: A Comparative Assessment of Smart Textiles-Related Applications. *Polymers* **2024**, *16*, 514. [CrossRef] [PubMed]
2. Dolgin, J.; Hanumantharao, S.N.; Farias, S.; Simon Jr, C.G.; Rao, S. Mechanical properties and morphological alterations in fiber-based scaffolds affecting tissue engineering outcomes. *Fibers* **2023**, *11*, 39. [CrossRef]
3. Ewaldz, E.; Rinehart, J.M.; Miller, M.; Brettmann, B. Processability of Thermoelectric Ultrafine Fibers via Electrospinning for Wearable Electronics. *ACS Omega* **2023**, *8*, 30239–30246. [CrossRef] [PubMed]
4. Cao, X.; Chen, W.; Zhao, P.; Yang, Y.; Yu, D.-G. Electrospun porous nanofibers: Pore-forming mechanisms and applications for photocatalytic degradation of organic pollutants in wastewater. *Polymers* **2022**, *14*, 3990. [CrossRef]
5. Li, L.; Chen, Z.; Pan, F.; Guo, H.; Wang, X.; Cheng, J.; Cai, L.; Xiu, Z.; Chen, L.; Batalu, D. Electrospinning technology on one dimensional microwave absorbers: Fundamentals, current progress, and perspectives. *Chem. Eng. J.* **2023**, *470*, 144236. [CrossRef]
6. Raza, Z.A.; Naeem, A.R.; Shafi, R.; Abid, S. Chitosan-incorporated poly (hydroxybutyrate) porous electrospun scaffold for potential biomedical applications. *Polym. Bull.* **2024**, *81*, 1691–1705. [CrossRef]
7. CeCe, R.; Jining, L.; Islam, M.; Korvink, J.G.; Sharma, B. An Overview of the Electrospinning of Polymeric Nanofibers for Biomedical Applications Related to Drug Delivery. *Adv. Eng. Mater.* **2024**, *26*, 2301297. [CrossRef]
8. Mtibe, A.; Muniyasamy, S.; Mokhena, T.C.; Ofosu, O.; Ojijo, V.; John, M. Recent insight into the biomedical applications of polybutylene succinate and polybutylene succinate-based materials. *Express Polym. Lett.* **2023**, *17*, 2–28. [CrossRef]
9. Farhaj, S.; Conway, B.R.; Ghorji, M.U. Nanofibres in drug delivery applications. *Fibers* **2023**, *11*, 21. [CrossRef]
10. Arroyo-Reyes, B.L.; Gómez-Muñoz, C.L.; Zaca-Morán, P.; Galindo-Ramírez, F.; Morales-Sánchez, M.A. Fabrication of a PLA/PVA-BIO-HA Polymeric Membrane by the Electrospinning Technique. *Fibers* **2024**, *12*, 33. [CrossRef]
11. Kesici Güler, H.; Cengiz Callioğlu, F. A new composite nanofibrous biomaterial development for drug delivery applications. *Express Polym. Lett.* **2023**, *17*, 487–501. [CrossRef]

12. Sell, S.A.; McClure, M.J.; Garg, K.; Wolfe, P.S.; Bowlin, G.L. Electrospinning of collagen/biopolymers for regenerative medicine and cardiovascular tissue engineering. *Adv. Drug Deliv. Rev.* **2009**, *61*, 1007–1019. [[CrossRef](#)] [[PubMed](#)]
13. Pina, S.; Oliveira, J.M.; Reis, R.L. Natural-based nanocomposites for bone tissue engineering and regenerative medicine: A review. *Adv. Mater.* **2015**, *27*, 1143–1169. [[CrossRef](#)] [[PubMed](#)]
14. Bhatia, S.; Bhatia, S. Natural polymers vs synthetic polymer. In *Natural Polymer Drug Delivery Systems*; Springer: Cham, Switzerland, 2016; pp. 95–118. [[CrossRef](#)]
15. Molnar, K.; Voniatis, C.; Feher, D.; Szabo, G.; Varga, R.; Reiniger, L.; Juriga, D.; Kiss, Z.; Krisch, E.; Weber, G.; et al. Poly(amino acid) based fibrous membranes with tuneable in vivo biodegradation. *PLoS ONE* **2021**, *16*, e0254843. [[CrossRef](#)]
16. Ray, S.S.; Bousmina, M. Biodegradable polymers and their layered silicate nanocomposites: In greening the 21st century materials world. *Prog. Mater. Sci.* **2005**, *50*, 962–1079. [[CrossRef](#)]
17. Gomez-Caturla, J.; Montanes, N.; Quiles-Carrillo, L.; Balart, R.; Garcia-Garcia, D.; Dominici, F.; Torre, L. Development of biodegradable PLA composites and tangerine peel flour with improved toughness containing a natural-based terpenoid. *Express Polym. Lett.* **2023**, *17*, 789–805. [[CrossRef](#)]
18. McClain, A.; Jindal, A.; Durr, H.; Puskas, J.E.; Leipzig, N.D. In Vivo Release of Zafirlukast from Electrospun Polyisobutylene-Based Fiber Mats to Reduce Capsular Contracture of Silicone Breast Prostheses. *ACS Appl. Bio Mater.* **2024**, *7*, 4442–4453. [[CrossRef](#)]
19. Biswas, M.C.; Jony, B.; Nandy, P.K.; Chowdhury, R.A.; Halder, S.; Kumar, D.; Ramakrishna, S.; Hassan, M.; Ahsan, M.A.; Hoque, M.E.; et al. Recent Advancement of Biopolymers and Their Potential Biomedical Applications. *J. Polym. Environ.* **2022**, *30*, 51–74. [[CrossRef](#)]
20. Molnar, K.; Varga, R.; Jozsa, B.; Barczikai, D.; Krisch, E.; Nagy, K.S.; Varga, G.; Jedlovsky-Hajdu, A.; Puskas, J.E. Investigation of the Cytotoxicity of Electrospun Polysuccinimide-Based Fiber Mats. *Polymers* **2020**, *12*, 2324. [[CrossRef](#)]
21. Li, G.; Zhao, M.; Xu, F.; Yang, B.; Li, X.; Meng, X.; Teng, L.; Sun, F.; Li, Y. Synthesis and biological application of polylactic acid. *Molecules* **2020**, *25*, 5023. [[CrossRef](#)]
22. Ilyas, R.A.; Zuhri, M.Y.M.; Aisyah, H.A.; Asyraf, M.R.M.; Hassan, S.A.; Zainudin, E.S.; Sapuan, S.M.; Sharma, S.; Bangar, S.P.; Jumaidin, R. Natural fiber-reinforced polylactic acid, polylactic acid blends and their composites for advanced applications. *Polymers* **2022**, *14*, 202. [[CrossRef](#)] [[PubMed](#)]
23. Kiss-Nagy, K.; Simongáti, G.; Ficzer, P. Investigation of 3D Printed Underwater Thruster Propellers Using CFD and Structural Simulations. *Period. Polytech. Mech. Eng.* **2024**, *68*, 70–77. [[CrossRef](#)]
24. Tábi, T.; Hajba, S. Cross effect of natural rubber and annealing on the properties of poly (lactic acid). *Period. Polytech. Mech. Eng.* **2019**, *64*, 270–277. [[CrossRef](#)]
25. Raquez, J.-M.; Habibi, Y.; Murariu, M.; Dubois, P. Polylactide (PLA)-based nanocomposites. *Prog. Polym. Sci.* **2013**, *38*, 1504–1542. [[CrossRef](#)]
26. Jacobsen, S.; Fritz, H.; Degée, P.; Dubois, P.; Jérôme, R. Polylactide (PLA)—A new way of production. *Polym. Eng. Sci.* **1999**, *39*, 1311–1319. [[CrossRef](#)]
27. Huang, C.; Thomas, N. Fabricating porous poly (lactic acid) fibres via electrospinning. *Eur. Polym. J.* **2018**, *99*, 464–476. [[CrossRef](#)]
28. Da Silva, D.; Kaduri, M.; Poley, M.; Adir, O.; Krinsky, N.; Shainsky-Roitman, J.; Schroeder, A. Biocompatibility, biodegradation and excretion of polylactic acid (PLA) in medical implants and theranostic systems. *Chem. Eng. J.* **2018**, *340*, 9–14. [[CrossRef](#)]
29. Kalita, N.K.; Nagar, M.K.; Mudenur, C.; Kalamdhad, A.; Katiyar, V. Biodegradation of modified Poly (lactic acid) based biocomposite films under thermophilic composting conditions. *Polym. Test.* **2019**, *76*, 522–536. [[CrossRef](#)]
30. Anderson, J.M.; Shive, M.S. Biodegradation and biocompatibility of PLA and PLGA microspheres. *Adv. Drug Deliv. Rev.* **1997**, *28*, 5–24. [[CrossRef](#)]
31. Luckachan, G.E.; Pillai, C. Biodegradable polymers—a review on recent trends and emerging perspectives. *J. Polym. Environ.* **2011**, *19*, 637–676. [[CrossRef](#)]
32. Park, T.G. Degradation of poly (D, L-lactic acid) microspheres: Effect of molecular weight. *J. Control. Release* **1994**, *30*, 161–173. [[CrossRef](#)]
33. Chen, V.J.; Ma, P.X. The effect of surface area on the degradation rate of nano-fibrous poly (L-lactic acid) foams. *Biomaterials* **2006**, *27*, 3708–3715. [[CrossRef](#)] [[PubMed](#)]
34. Hurrell, S.; Cameron, R.E. The effect of initial polymer morphology on the degradation and drug release from polyglycolide. *Biomaterials* **2002**, *23*, 2401–2409. [[CrossRef](#)] [[PubMed](#)]
35. Park, T.G. Degradation of poly (lactic-co-glycolic acid) microspheres: Effect of copolymer composition. *Biomaterials* **1995**, *16*, 1123–1130. [[CrossRef](#)]
36. Leonés, A.; Peponi, L.; Lieblisch, M.; Benavente, R.; Fiori, S. In vitro degradation of plasticized PLA electrospun fiber mats: Morphological, thermal and crystalline evolution. *Polymers* **2020**, *12*, 2975. [[CrossRef](#)]
37. Xu, X.; Chen, X.; Wang, Z.; Jing, X. Ultrafine PEG–PLA fibers loaded with both paclitaxel and doxorubicin hydrochloride and their in vitro cytotoxicity. *Eur. J. Pharm. Biopharm.* **2009**, *72*, 18–25. [[CrossRef](#)]

38. Yuan, X.; Mak, A.F.T.; Yao, K. Comparative observation of accelerated degradation of poly(l-lactic acid) fibres in phosphate buffered saline and a dilute alkaline solution. *Polym. Degrad. Stab.* **2002**, *75*, 45–53. [[CrossRef](#)]
39. You, Y.; Min, B.M.; Lee, S.J.; Lee, T.S.; Park, W.H. In vitro degradation behavior of electrospun polyglycolide, polylactide, and poly (lactide-co-glycolide). *J. Appl. Polym. Sci.* **2005**, *95*, 193–200. [[CrossRef](#)]
40. Bogdanova, A.; Pavlova, E.; Polyanskaya, A.; Volkova, M.; Biryukova, E.; Filkov, G.; Trofimenko, A.; Durymanov, M.; Klinov, D.; Bagrov, D. Acceleration of electrospun PLA degradation by addition of gelatin. *Int. J. Mol. Sci.* **2023**, *24*, 3535. [[CrossRef](#)]
41. Dias, J.C.; Ribeiro, C.; Sencadas, V.; Botelho, G.; Ribelles, J.G.; Lanceros-Méndez, S. Influence of fiber diameter and crystallinity on the stability of electrospun poly (l-lactic acid) membranes to hydrolytic degradation. *Polym. Test.* **2012**, *31*, 770–776. [[CrossRef](#)]
42. Zong, X.; Ran, S.; Kim, K.-S.; Fang, D.; Hsiao, B.S.; Chu, B. Structure and Morphology Changes during in Vitro Degradation of Electrospun Poly(glycolide-co-lactide) Nanofiber Membrane. *Biomacromolecules* **2003**, *4*, 416–423. [[CrossRef](#)] [[PubMed](#)]
43. Li, P.; Feng, X.; Jia, X.; Fan, Y. Influences of tensile load on in vitro degradation of an electrospun poly (l-lactide-co-glycolide) scaffold. *Acta Biomater.* **2010**, *6*, 2991–2996. [[CrossRef](#)] [[PubMed](#)]
44. Mujica-Garcia, A.; Navarro-Baena, I.; Kenny, J.M.; Peponi, L. Influence of the processing parameters on the electrospinning of biopolymeric fibers. *J. Renew. Mater.* **2014**, *2*, 23–34. [[CrossRef](#)]
45. Zubir, A.A.M.; Khairunnisa, M.; Surib, N.A.; NorRuwaida, J.; Rashid, M. Electrospinning of PLA with DMF: Effect of polymer concentration on the bead diameter of the electrospun fibre. In *IOP Conference Series: Materials Science and Engineering*; IOP Publishing: Bristol, UK, 2020; p. 012087.
46. Fischer, E.; Sterzel, H.J.; Wegner, G. Investigation of the structure of solution grown crystals of lactide copolymers by means of chemical reactions. *Kolloid-Z. Und Z. Für Polym.* **1973**, *251*, 980–990. [[CrossRef](#)]
47. Thompson, C.; Chase, G.G.; Yarin, A.; Reneker, D. Effects of parameters on nanofiber diameter determined from electrospinning model. *Polymer* **2007**, *48*, 6913–6922. [[CrossRef](#)]
48. Casasola, R.; Thomas, N.L.; Trybala, A.; Georgiadou, S. Electrospun poly lactic acid (PLA) fibres: Effect of different solvent systems on fibre morphology and diameter. *Polymer* **2014**, *55*, 4728–4737. [[CrossRef](#)]
49. Gajjar, C.R.; King, M.W. *Resorbable Fiber-Forming Polymers for Biotextile Applications*; Springer: Berlin/Heidelberg, Germany, 2014.
50. Kost, B.; Basko, M.; Bednarek, M.; Socka, M.; Kopka, B.; Łapienis, G.; Biela, T.; Kubisa, P.; Brzeziński, M. The influence of the functional end groups on the properties of polylactide-based materials. *Prog. Polym. Sci.* **2022**, *130*, 101556. [[CrossRef](#)]
51. Kuzelova Kostakova, E.; Meszaros, L.; Maskova, G.; Blazkova, L.; Turcsan, T.; Lukas, D. Crystallinity of Electrospun and Centrifugal Spun Polycaprolactone Fibers: A Comparative Study. *J. Nanomater.* **2017**, *2017*, 8952390. [[CrossRef](#)]
52. Laramée, A.W.; Pellerin, C. Raman Analysis of Orientation and Crystallinity in High Tg, Low Crystallinity Electrospun Fibers. *Appl. Spectrosc.* **2023**, *77*, 1289–1299. [[CrossRef](#)]
53. Szabó, E.; Záhonyi, P.; Brecka, D.; Galata, D.L.; Mészáros, L.A.; Madarász, L.; Csorba, K.; Vass, P.; Hirsch, E.; Szafraniec-Szczęsny, J.; et al. Comparison of Amorphous Solid Dispersions of Spirolactone Prepared by Spray Drying and Electrospinning: The Influence of the Preparation Method on the Dissolution Properties. *Mol. Pharm.* **2020**, *18*, 317–327. [[CrossRef](#)]
54. D’Amato, A.R.; Bramson, M.T.; Corr, D.T.; Puhl, D.L.; Gilbert, R.J.; Johnson, J. Solvent retention in electrospun fibers affects scaffold mechanical properties. *Electrospinning* **2018**, *2*, 15–28. [[CrossRef](#)] [[PubMed](#)]
55. Larrañaga, A.; Lizundia, E. A review on the thermomechanical properties and biodegradation behaviour of polyesters. *Eur. Polym. J.* **2019**, *121*, 109296. [[CrossRef](#)]
56. Aharoni, S.M. Increased glass transition temperature in motionally constrained semicrystalline polymers. *Polym. Adv. Technol.* **1998**, *9*, 169–201. [[CrossRef](#)]
57. Lin, Y.; Zhang, K.-Y.; Dong, Z.-M.; Dong, L.-S.; Li, Y.-S. Study of Hydrogen-Bonded Blend of Polylactide with Biodegradable Hyperbranched Poly(ester amide). *Macromolecules* **2007**, *40*, 6257–6267. [[CrossRef](#)]
58. Tamburini, G.; Bertagnoli, S.; Tarricone, G.; Piva, S.; Sassella, A.; Lorenzi, R.; Paleari, A. Early stages of X-ray induced molecular unit modifications in poly(lactic acid). *Polym. Degrad. Stab.* **2023**, *216*, 110485. [[CrossRef](#)]
59. Lee, H.W.; Insyani, R.; Prasetyo, D.; Prajitno, H.; Sitompul, J. Molecular Weight and Structural Properties of Biodegradable PLA Synthesized with Different Catalysts by Direct Melt Polycondensation. *J. Eng. Technol. Sci.* **2015**, *47*, 364–373. [[CrossRef](#)]
60. Agarwal, M.; Koelling, K.W.; Chalmers, J.J. Characterization of the Degradation of Polylactic Acid Polymer in a Solid Substrate Environment. *Biotechnol. Progr.* **1998**, *14*, 517–526. [[CrossRef](#)]
61. Kister, G.; Cassanas, G.; Vert, M. Effects of morphology, conformation and configuration on the IR and Raman spectra of various poly(lactic acid)s. *Polymer* **1998**, *39*, 267–273. [[CrossRef](#)]
62. Garlotta, D. A Literature Review of Poly(Lactic Acid). *J. Polym. Environ.* **2001**, *9*, 63–84. [[CrossRef](#)]
63. Vargas-Villagran, H.; Romo-Urbe, A.; Teran-Salgado, E.; Dominguez-Diaz, M.; Flores, A. Electrospun polylactic acid non-woven mats incorporating silver nanoparticles. *Polym. Bull.* **2014**, *71*, 2437–2452. [[CrossRef](#)]
64. del Rosario Salazar-Sánchez, M.; Campo-Erazo, S.D.; Villada-Castillo, H.S.; Solanilla-Duque, J.F. Structural changes of cassava starch and polylactic acid films submitted to biodegradation process. *Int. J. Biol. Macromol.* **2019**, *129*, 442–447. [[CrossRef](#)]

65. Tsuji, H.; Ikada, Y. Properties and morphology of poly (L-lactide) 4. Effects of structural parameters on long-term hydrolysis of poly (L-lactide) in phosphate-buffered solution. *Polym. Degrad. Stab.* **2000**, *67*, 179–189. [[CrossRef](#)]
66. Vaid, R.; Yildirim, E.; Pasquinelli, M.A.; King, M.W. Hydrolytic degradation of polylactic acid fibers as a function of ph and exposure time. *Molecules* **2021**, *26*, 7554. [[CrossRef](#)] [[PubMed](#)]

**Disclaimer/Publisher’s Note:** The statements, opinions and data contained in all publications are solely those of the individual author(s) and contributor(s) and not of MDPI and/or the editor(s). MDPI and/or the editor(s) disclaim responsibility for any injury to people or property resulting from any ideas, methods, instructions or products referred to in the content.